HAL open science

STEREO database of interplanetary Langmuir electric waveforms

Carine Briand, Pierre Henri, V. Génot, N. Lormant, N. Dufourg, B. Cecconi, Q. N. Nguyen, K. Goetz

To cite this version:

Carine Briand, Pierre Henri, V. Génot, N. Lormant, N. Dufourg, et al.. STEREO database of interplanetary Langmuir electric waveforms. Journal of Geophysical Research Space Physics, 2016, 121 (2), pp.1062-1070. ⟨10.1002/2015JA022036⟩. ⟨hal-01311872⟩

HAL Id: hal-01311872

https://hal.sorbonne-universite.fr/hal-01311872v1

Submitted on 4 May 2016

HAL is a multi-disciplinary open access archive for the deposit and dissemination of scientific research documents, whether they are published or not. The documents may come from teaching and research institutions in France or abroad, or from public or private research centers.

L'archive ouverte pluridisciplinaire **HAL**, est destinée au dépôt et à la diffusion de documents scientifiques de niveau recherche, publiés ou non, émanant des établissements d'enseignement et de recherche français ou étrangers, des laboratoires publics ou privés.

Autorisation HAL

HAL Authorization

AGU PUBLICATIONS

JGR

Journal of Geophysical Research: Space Physics

TECHNICAL REPORTS: DATA

10.1002/2015JA022036

Key Points:

- This paper describes a database of Langmuir/Z-mode waveforms, available at the CDPP
- The Langmuir waveforms were recorded by the WAVES/TDS instrument on board the STEREO mission
- The peak amplitude distribution of 11,675 Langmuir/Z-mode waves is also analyzed

Correspondence to:
C. Briand,
carine.briand@obspm.fr

Citation:
Briand, C., P. Henri, V. Génot, N. Lormant, N. Dufourg, B. Cecconi, Q. N. Nguyen, and K. Goetz (2016), STEREO database of interplanetary Langmuir electric waveforms, *J. Geophys. Res. Space Physics*, *121*, 1062–1070, doi:10.1002/2015JA022036.

Received 14 OCT 2015
Accepted 7 JAN 2016
Accepted article online 14 JAN 2016
Published online 6 FEB 2016

©2016. American Geophysical Union. All Rights Reserved.

STEREO database of interplanetary Langmuir electric waveforms

C. Briand[1], P. Henri[2], V. Génot[3], N. Lormant[4], N. Dufourg[5], B. Cecconi[1], Q. N. Nguyen[1], and K. Goetz[6]

[1]LESIA, Observatoire de Paris, CNRS, UPMC, University Paris Diderot, Meudon, France, [2]LPC2E, CNRS, Orléans University, Orléans, France, [3]IRAP, CNRS, Université Paul Sabatier, Toulouse, France, [4]AKKA Technologies, Toulouse, France, [5]CNES, Toulouse, France, [6]School of Physics and Astronomy, University of Minnesota, Minneapolis, Minnesota, USA

Abstract This paper describes a database of electric waveforms that is available at the Centre de Données de la Physique des Plasmas (CDPP, http://cdpp.eu/). This database is specifically dedicated to waveforms of Langmuir/Z-mode waves. These waves occur in numerous kinetic processes involving electrons in space plasmas. Statistical analysis from a large data set of such waves is then of interest, e.g., to study the relaxation of high-velocity electron beams generated at interplanetary shock fronts, in current sheets and magnetic reconnection region, the transfer of energy between high and low frequencies, the generation of electromagnetic waves. The Langmuir waveforms were recorded by the Time Domain Sampler (TDS) of the WAVES radio instrument on board the STEREO mission. In this paper, we detail the criteria used to identify the Langmuir/Z-mode waves among the whole set of waveforms of the STEREO spacecraft. A database covering the November 2006 to August 2014 period is provided. It includes electric waveforms expressed in the normalized frame $(B, B\times V_{sw}, B\times(B\times V_{sw}))$ with B and V_{sw} the local magnetic field and solar wind velocity vectors, and the local magnetic field in the variance frame, in an interval of $\pm$1.5 min around the time of the Langmuir event. Quicklooks are also provided that display the three components of the electric waveforms together with the spectrum of $E_{\parallel}$, together with the magnitude and components of the magnetic field in the 3 min interval, in the variance frame. Finally, the distribution of the Langmuir/Z-mode waves peak amplitude is also analyzed.

1. Introduction

Langmuir waves are ubiquitous in the interplanetary medium and planetary environments, from the solar wind to the ionosphere of the planets, their foreshock and even cometary tails (see an extended review in *Briand* [2015]). They correspond to the collective oscillation of electrons close to the plasma frequency over a fixed, neutralizing positive ion background. Being closely related to the electrons dynamics, they allow us to deduce some particles' properties. Thermal Langmuir waves provide a tool to determine the plasma density and temperature, through quasi-thermal noise spectroscopy method [*Meyer-Vernet and Perche*, 1989]. Langmuir wave observations have also allowed us to cross calibrate particle data when spectroscopy was not available [*Opitz et al.*, 2010]. Also, higher-amplitude waves can be used to determine density fluctuations at a frequency range difficult to achieve with particle instruments [*Malaspina et al.*, 2010; *Henri et al.*, 2011]. Such measurements are crucial for studies of electrostatic turbulence. High-amplitude Langmuir waves also reveal the presence of suprathermal electron beams. Through wave coupling, they are at the origin of electromagnetic radiation, among the most intense of the solar radio emission spectrum (called Type II and Type III bursts) and other fainter radiations of the solar spectrum [*Briand et al.*, 2008]. Finally, in a collisionless plasma, they facilitate energy exchange between species of different inertia (typically between electrons and protons), through nonlinear wave coupling.

Due to their electrostatic nature, Langmuir waves can only be observed in situ. Several space missions have provided different measurements around the plasma frequency, i.e., in the Langmuir wave frequency range. Cassini RPWS/WFR and RPWS/WBR [*Gurnett et al.*, 2004] and Cluster WBD Plasma Wave Receiver [*Gurnett et al.*, 1997] are mostly dedicated to magnetospheric observations of Saturn and the Earth, respectively, even if some measurements were also obtained in the free (i.e., not magnetically connected to the planet) solar wind. Ulysses/URAP [*Stone et al.*, 1992] and WIND/WAVES [*Bougeret et al.*, 1995] observed mostly in the free solar wind (with some excursions in the Earth magnetosphere, in particular, in the early phase of the mission). While Ulysses provided only spectral information, WIND is equipped with a Time Domain Sampler (TDS)

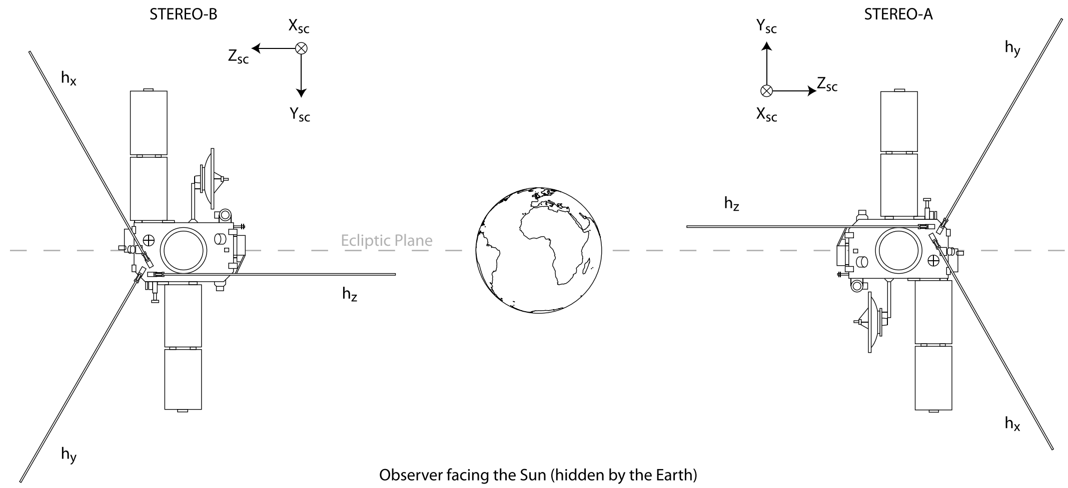

Figure 1. STEREO antenna orientation as seen from an observer facing the Sun (hidden by the Earth in the scheme). $h_{x,y,z}$ display the physical antenna, while $(X,Y,Z)_{sc}$ shows the orientation of the spacecraft reference frame.

measuring electric field waveforms. Finally, STEREO/WAVES [*Bougeret et al.*, 2008] (see the description below) has been providing spectral and waveform data mostly in the solar wind at about 0.95 AU (STEREO A) and 1.03 AU (STEREO B). Note that except Ulysses, the other missions are located in a plane close to the ecliptic. In the future, Solar Orbiter (launch foreseen in 2018) should provide new measurements at higher latitudes ($\pm 30°$ from the ecliptic). Also, Solar Probe + (launch foreseen for 2018) will explore unknown areas while approaching the Sun down to about nine solar radii above the solar surface.

Spectral instruments allow a continuous detection of the waves at the expense of the spectral resolution and a loss of information on the wave's phase. Conversely, waveform instruments provide a limited temporal (approximately seconds per day) and spectral (approximately tens of kHz) coverage, but the data have a much better spectral resolution and the phase information on the waves is retained. This allows to test the fundamental laws of physical processes such as linear waves interactions [see, e.g., *Henri et al.*, 2009].

Section 2 presents the instruments and data used to build the database. Then, section 3 details the information and format of the data in the database and presents the interface used to access the data. Finally, section 4 displays some analysis of the data (in particular, the distribution of the peak amplitude of the wave).

2. Observations

The STEREO mission is composed of two nearly identical spacecraft, one orbiting ahead of the Earth (STEREO A) and the other behind (STEREO B). During the early stage of the mission (2006 and first three months of 2007), the spacecraft explored the Earth environment (in particular, the Earth foreshock). Then, they were sufficiently separated to be in the non-Earth-connected solar wind environment. The STEREO platform is three-axis stabilized, always pointing its optical instruments toward the Sun. The radio instrument (WAVES) is composed of three orthogonal, monopole antennas (Figure 1), located at the back (away from the Sun) of the probe, and a series of observing modes working simultaneously:

1. a spectrum analyzer providing continuous spectrum on three channels covering the range 2.5 kHz to 16 MHz;

Table 1. Available Filters for the TDS Instruments[a]

Filter Name	Sample Speed (s/s)	Low-Pass Filter (kHz)	Maximum Duration (ms)
A	250,000	108	66
B	125,000	54	131
C	31,250	13.5	524
D	7,812.5	3.375	2097

[a]From *Bougeret et al.* [2008].

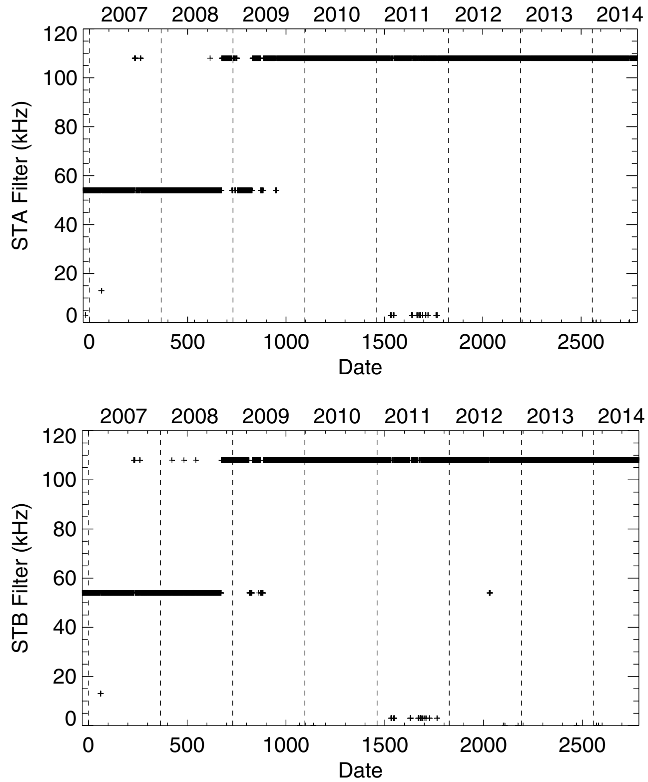

Figure 2. Daily configuration of the filter for (top) STA and (bottom) STB. The bottom axis of each figure displays the number of days from 1 January 2007, while the top axis indicates the year, delimited by the vertical dashed lines.

2. a Low Rate Science (LRS) providing electric field and density measurements in the low-frequency range of the spectrum;
3. a Langmuir Waves Statistics (LWS) mode providing the distribution of the peak intensity of the waves observed by TDS; from 28 September 2007, the peak intensity is deduced every 40 ms and a distribution is built every 10 min; and
4. a Time Domain Sampler (TDS) that delivers about 40 electric waveforms per day. The range of frequency depend on the filter configuration (see Table 1).

The configuration of the TDS mode has been changed several times during the period analyzed here: Figure 2 displays the daily filter configuration for each spacecraft. Only the configuration with the filters A, B, and C allows the detection of the high-frequency waves (Langmuir waves have a typical frequency of 20 kHz at 1 AU, see Figure 6). About 40 waveforms are transmitted to the ground daily. They correspond not only to waveforms of high amplitude but also to randomly selected events (i.e., not specifically intense waves). This means that about 10^5 waveforms were recorded in the time interval considered here (November 2006 to August 2014).

The analysis of the waveforms also requires several other parameters of the solar wind. In particular, the magnetic field and the solar wind velocity vectors are obtained from the 8Hz resolution data of the IMPACT/MAG experiment [*Luhmann et al.*, 2008] and the 1 min resolution data of PLASTIC [*Galvin et al.*, 2008] respectively.

3. Database Description

The data set is composed of two CDF files containing the data and a probability density function (PDF) file with some graphs.

3.1. Electric Field: Waveforms and Spectrum

The database was built from a comprehensive analysis of the electric waveforms observed by STEREO/WAVES-TDS from 1 November 2006 (i.e., a few days after the launch) until 20 August 2014. After this date, the signal with the probes was lost as they passed behind the Sun. Langmuir waves are pure electrostatic waves. In some cases, a nonnegligible perpendicular component is observed. These waves are interpreted in terms

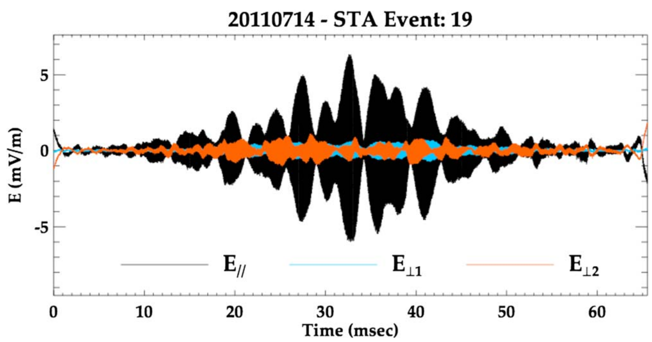

Figure 3. Example of electric waveform expressed in the physical frame coordinate discussed in the text. The field is expressed in mV/m. The top title of the figure indicates the date of the event, the spacecraft that observed it (STA or STB), and the event number of the day. As expected for Langmuir waves, the field is almost aligned with the local magnetic field: the $E_{\|}$ component dominates.

of Z-mode, i.e., an electromagnetic waves at about the plasma frequency. Indeed, taking into account the weak magnetization of the plasma, the Langmuir dispersion branch is continuously connected to the Z-mode, which may lead to oblique propagation of waves close to the plasma frequency [*Briand et al.*, 2010; *Graham and Cairns*, 2013]. Both Langmuir and Z-mode waves constitute the data set.

To detect the Langmuir/Z-mode events, we first determine the spectrum of the *x* component of the electric field (spacecraft coordinates, using the W/base caps (Graz) conversion factors [*Bale et al.*, 2008] see Figure 1).

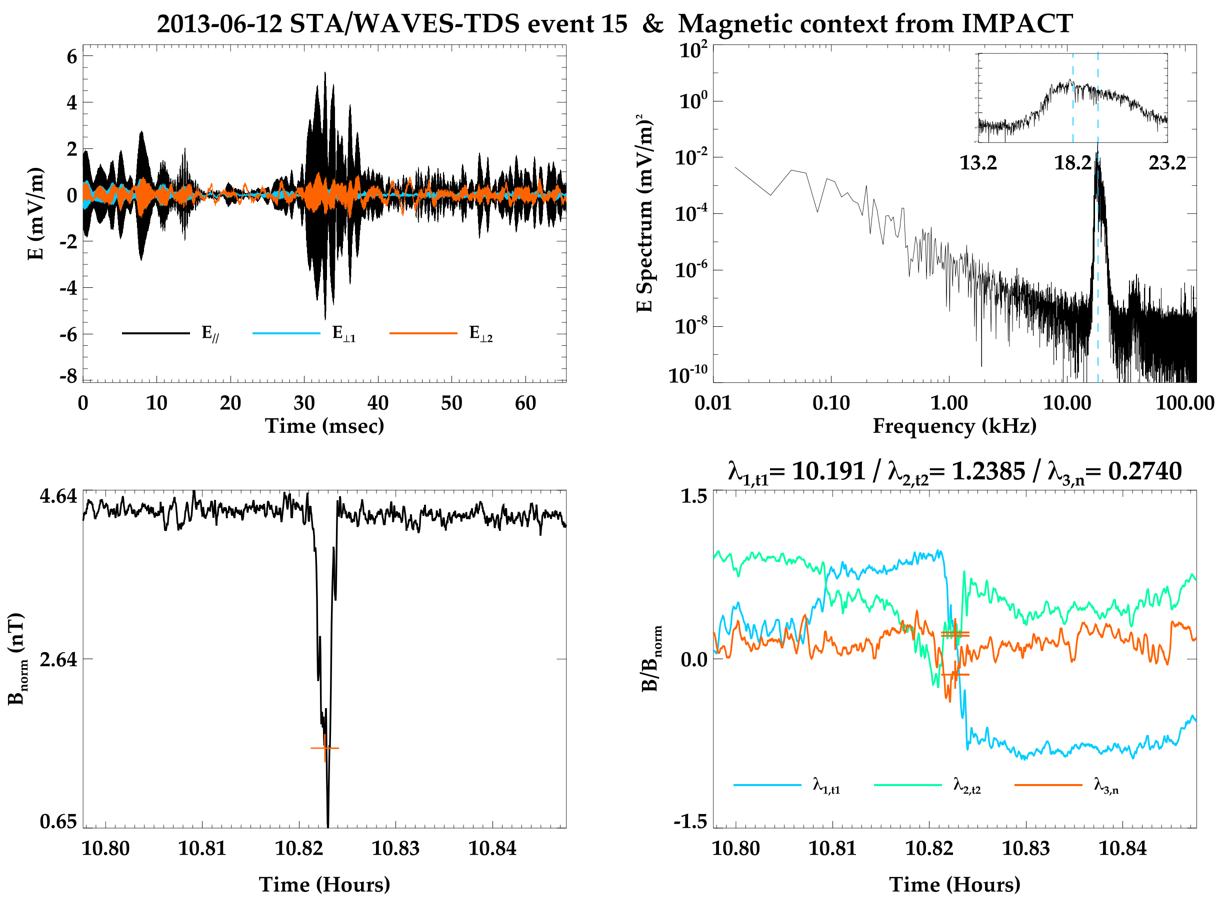

Figure 4. Example of a quicklook distributed with the data. The four panels display (top left) the three components of the electric field, (top right) the electric spectrum, (bottom left) the norm of the magnetic field in a 3 min window interval, and (bottom right) the (normalized) components of the magnetic field. In Figures 4 (bottom left) and 4 (bottom right), the red cross indicates the time when the Langmuir event was detected. On Figure 4 (bottom right), the maximum, intermediate, and minimum eigenvalues are indicated.

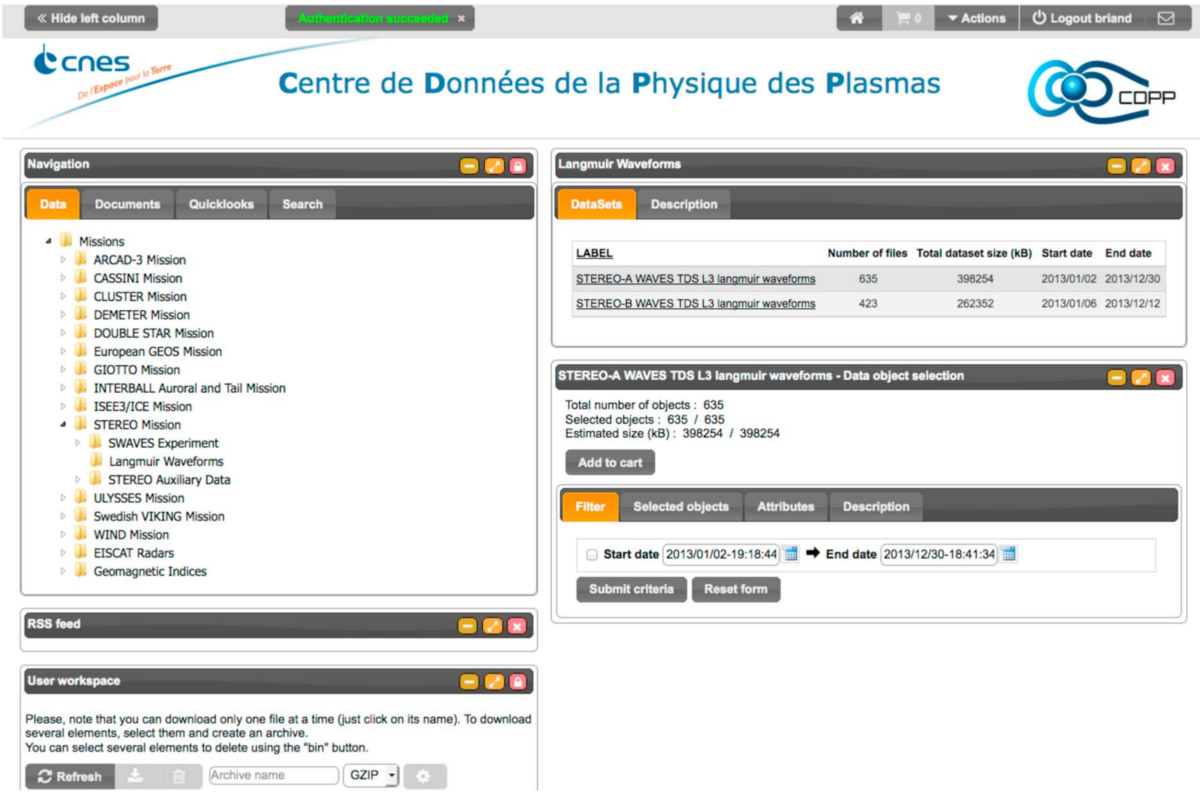

Figure 5. User interface to access the data (https://cdpp-archive.cnes.fr/). The "Navigation" (left) side allows to select the data set to explore, either from the "Data" or from the Quicklooks tabs. The right side of the interface is specific to the selected data set. Here two data sets are available, one for each spacecraft. The bottom right panel (labeled "Data object selection") allows one to select the data.

Then, the peak is detected and a Gaussian is fitted around this position. In case of multiple peaks, the one with the largest amplitude is considered. The signal is identified as a Langmuir/Z-mode wave if the following criteria are satisfied:

1. The position of the electric power spectrum peak falls in the range 5 to 50 kHz; the lower limit keeps low-density events at the expense of increasing false detections, e.g., the signature of ion acoustic waves or ion-bulk waves [*Vecchio et al.*, 2014; *Valentini et al.*, 2014];
2. The width around the peak frequency must be sharp enough. Specifically, the sigma of the Gaussian fit around the peak must be lower than $5 \times 10^{-2} f_p$. This allows us to distinguish between the low-frequency signals (which display large bandwidth) and the Langmuir/Z-mode ones;
3. The peak must be at least 10 dB above the background level;

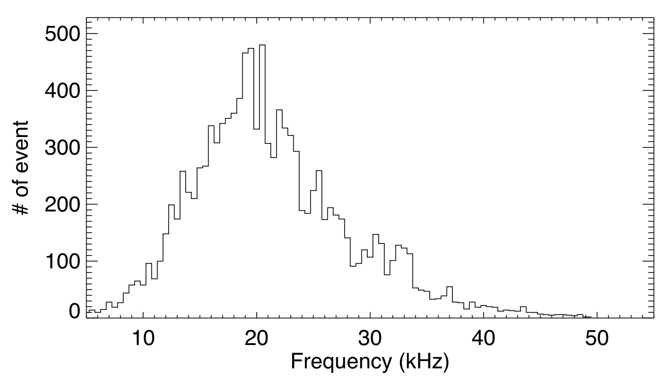

Figure 6. Histogram of the Langmuir event frequencies.

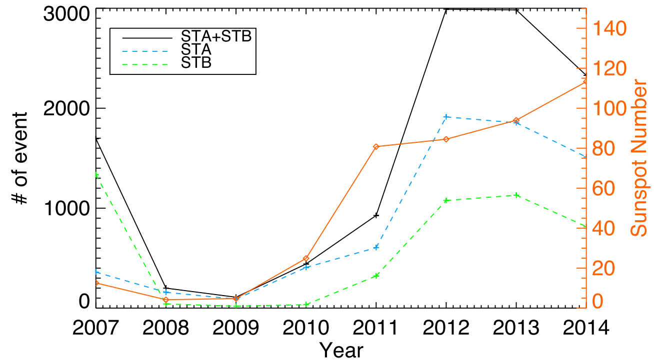

Figure 7. Number of Langmuir events detected each year. The black curve corresponds to the sum of events from satellite A (STA) and B (STB), while the two color curves display the number of events detected by each spacecraft separately. Superimposed yearly sunspot number as given by the SIDC (red axis).

4. The signal must be sufficiently far from the upper frequency limit of each filter. A value of $0.9f_{upper}$ is used. This condition was particularly necessary for C filter data (see Table 1) to limit the confusion with low-frequency, non-Langmuir signal; and
5. The peak intensity should fall outside the 15.61 – 15.64 kHz frequency range, which has spurious signal of instrumental origin;

False detections remain, but we estimate that they represent less than 1% of the total data set. Instead of restricting the selection criteria further, which could lead to the rejection of too many true events, we have preferred to accept this level of false detection. Moreover, being easily identified visually, they can be rejected during later analysis: a visual inspection of the data set was performed to remove possible bad identifications.

Once the waveforms have been selected, they are projected from the spacecraft frame into a more physical coordinate system. We thus rotate the data into the normalized coordinate frame: $(\frac{\mathbf{B}}{\|\mathbf{B}\|}, \frac{\mathbf{B}\times\mathbf{V}_{sw}}{\|\mathbf{B}\times\mathbf{V}_{sw}\|}, \frac{\mathbf{B}\times(\mathbf{B}\times\mathbf{V}_{sw})}{\|\mathbf{B}\times(\mathbf{B}\times\mathbf{V}_{sw})\|})$. Here **B** and $\mathbf{V}_{sw}$ are the magnetic field and the solar wind velocity vector at the time of the Langmuir event, respectively, in spacecraft coordinates. For missing values of solar wind velocity the vector [−1,0,0] is imposed. The component of the electric field are thus parallel and perpendicular to the local magnetic field ($E_{\|}, E_{\perp 1}, E_{\perp 2}$). An example is shown on Figure 3.

3.2. Magnetic Field Contextual Information

Some additional information on the magnetic context of the Langmuir/Z-mode events complement each electric field measurement. We indeed provide another CDF file with the magnetic field in spacecraft and variance coordinates, in a 3 min interval around the Langmuir event time (i.e., ±1.5 min around the event). The

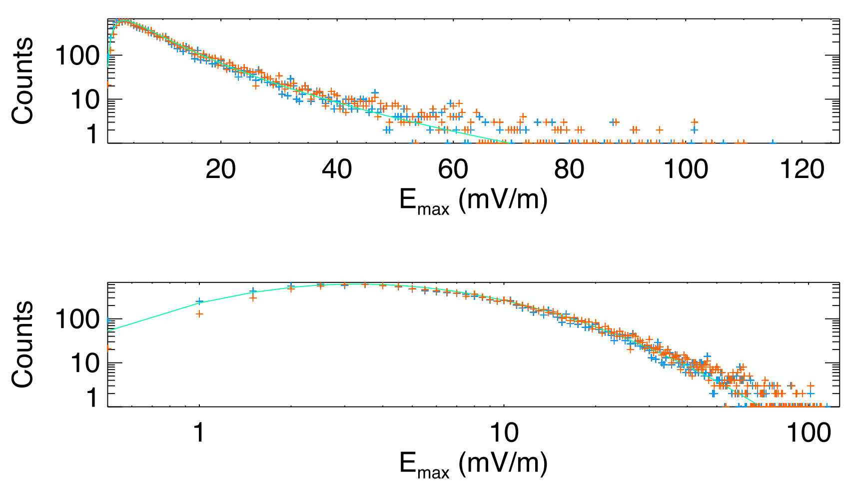

Figure 8. Histogram of the maximum amplitude of the waveforms. The blue crosses display the distribution of $E_{\|}^{max}$, while the red crosses display the distribution of E^{max}. The green line is the lognormal fit with the parameters given in the text. The bin size is 0.5 mV/m.

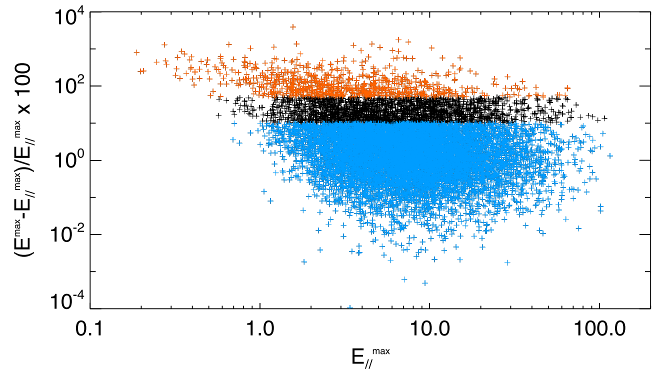

Figure 9. *R* versus $E_{\parallel}^{max}$ (in mV/m). The blue crosses display the events with $R \leq 10$, the red crosses display the events with $R \geq 50$.

variance coordinates [*Sonnerup and Scheible*, 1998; *Khrabrov and Sonnerup*, 1998] allow us to catch different magnetic jump signatures (e.g., period of interplanetary shocks, magnetic holes, and current sheet regions). The results of a variance analysis are strongly dependent on the chosen time interval. The 3 min interval has proven a good compromise to keep most of the magnetic configuration. To estimate the analysis quality, the three eigenvalues related to the minimum, intermediate, and maximum eigenvectors are indicated. The magnetic field is also provided in spacecraft coordinates, in case the variance analysis results are meaningless.

3.3. Quicklook

The quicklooks distributed together with the data display the following:

1. the three components of the electric field ($E_{\parallel}, E_{\perp 1}, E_{\perp 2}$) (Figure 4, top left);
2. the power spectrum of the $E_{\parallel}$ component in the range 0.01 – 130 kHz, with an enlarged view of 10 kHz around the peak value (Figure 4, top right);
3. the norm of the magnetic field in nanoteslas (Figure 4, bottom left); and
4. the three components of the magnetic field in the variance frame (Figure 4, bottom right). The eigenvalues are also indicated to judge the quality of the variance analysis.

The quicklooks are provided in a PDF format. The file name also contains information on the event number of that day (as labelled in the original STEREO data).

3.4. Access to the Data

The CDPP (Centre de Données de la Physique des Plasmas) is the French national center for space physics data. It was jointly created by CNES (Centre National d'Etudes Spatiales) and CNRS (Centre National de la Recherche Scientifique) in 1998; it is hosted at IRAP (Institut de Recherche Atmosphérique et Planétaire, Toulouse). The database is accessible from the website: https://cdpp-archive.cnes.fr/ . The access is free but requires a temporary or permanent account. A specific "registration button" is available from the interface to request such an account. Once logged in, you can select the data set through the "Navigation" column (see Figure 5), under the "Data" or "Quicklooks" tab (depending if you want to access the data themselves or just the quicklooks). The right part of the interface then displays information, specific to the selected data set. In our case, selecting "STEREO/Langmuir Waveforms" from the Navigation tab, the interface shows the two available data sets (one for each spacecraft). When we select one of them, a "Data object selection" panel allows us to select the waveform from their date of occurrence.

Once the data are selected through the CDPP interface, a zip file is generated that contains (a) the plot of the data in PDF format, (b) the electric waveform in a CDF file, and (c) the magnetic field context in a separated CDF file. The name of the file is as follow: st#_l2_*TTT*_lang_*YYYYMMDD_HHMMSS*_v01.cdf, with # as the name of the spacecraft (A or B), *TTT* the name of the data type (tds or mag for the TDS or magnetic field data), the date and time. The label "l2" refers to the data level treatment. The version number of the file is indicated at the end of the file name. This zip file is then available for download through your user workspace. For more information and help regarding the interface, use the "email" button on the top right side of the interface.

4. Discussion and Conclusions

In this paper we have described a database of Langmuir events obtained from records of the STEREO mission. Among the about 10^5 waveforms observed by the two STEREO spacecraft, 11,675 correspond to Langmuir/Z-mode events and constitute our database. The frequency histogram (Figure 6) shows that the choice of the frequency limits for the detection (5 – 50 kHz) correctly covers the range of observed frequencies.

As can be seen from Figure 7 the number of events strongly depends on the phase of the solar cycle: the number of event increases as the solar activity increases. This is indeed expected as the formation of the Langmuir waves is linked to the launch of electron beams in the interplanetary medium, which is a common consequence of an increase of the solar activity. More, unexpectedly, the number of events is larger on STA than in STB, by a factor of about 2. This may be due to a larger number of nanodust particles detected by TDS on STEREO B while the number of events per day is fixed.

The distribution of the envelope electric field of the waves provides clues on the generation processes of the waves (see the detailed discussion in *Nulsen et al.* [2007, and references therein). In particular, as developed in the Stochastic Growth Theory [*Robinson*, 1995], when Langmuir waves grow in an inhomogeneous medium, where thermal and nonlinear effects are negligible, the growth rate varies randomly (following the encountered density and temperature conditions), leading to a lognormal distribution of the logarithm of the electric field envelope. Deviation from such a distribution thus stresses the importance of thermal and nonlinear effects.

Our database provides a large number of samples from which we can build the distribution of the maximum amplitude of the Langmuir wave. We have thus built the distribution of the maxima of the (absolute value) parallel component $E_{\parallel}^{\max}$, the perpendicular components being negligible for Langmuir waves. It is displayed with blue crosses in Figure 8. However, our database also contains events with large perpendicular components. When displaying the parallel component only, we cannot distinguish between pure parallel polarized waves or more elliptical ones. To estimate the contribution of the elliptically polarized waves (i.e., non-Langmuir waves) to the $E_{\parallel}^{\max}$ distribution, we have built the distribution of the maximum of the amplitude of E, $E^{\max}=\max\left(\sqrt{E_{\parallel}^2+E_{\perp 1}^2+E_{\perp 2}^2}\right)$. If the wave is a Langmuir wave $E^{\mathrm{Max}} \approx E_{\parallel}^{\max}$ since the wave is mostly parallel to the magnetic field. As the waves have more pronounced perpendicular components, the $E^{\max}$ becomes much larger than $E_{\parallel}^{\max}$. The spurious low-frequency fluctuations have been filtered out from the data. The distribution of E^{Max} is displayed in red on Figure 8. It is important to remember that the two distributions take into account all the events in the database, irrespective of environment (Type II or III, magnetic holes, etc.) or solar wind conditions (pressure, velocity, etc.).

The distribution of $E_{\parallel}^{\mathrm{Max}}$ have been fitted with a lognormal function:

$$P(\log_{10} E) = \frac{A}{\sigma\sqrt{2\pi}} \exp\left(\frac{\left(\log_{10} E_{\max} - \mu\right)^2}{2\sigma^2}\right) \tag{1}$$

For the $E_{\parallel}^{\max}$ distribution, the following parameters have been obtained: $\sigma = 0.37 \pm 0.01$ and $\mu =< \log_{10} E_{max} > = 3.30 \pm 0.05$ A is a normalization factor. As can be verified in Figure 8, the fit is very good for waves amplitude below 10 mV/m, while departure from the lognormal law is large above 30 mV/m. This suggests that thermal and nonlinear effects play a more dominant role for large amplitude waves, as expected. Note that above 60 mV/m the number of counts in each bin is very low. The discrepancy observed at low intensity on $E^{\max}$ stresses the fact that for these events the perpendicular components contribute as much as the parallel one to the amplitude of the electric field (but not necessarily with a peak around the plasma frequency).

Another way to quantify the contribution of the perpendicular component waves to the distribution is to define the ratio:

$$R = \frac{E^{\max} - E_{\parallel}^{\max}}{E_{\parallel}^{\max}} \times 100. \tag{2}$$

R is close to zero when the contribution of the perpendicular components is negligible and takes larger values when it is of the same order or is dominant compared to the parallel component. The Figure 9 dispays *R* versus $E_{\parallel}^{max}$. The contribution of the perpendicular components at low amplitude is quite large (explaining

Acknowledgments
The STEREO/WAVES instrument was designed, built, and is operated by teams at Paris Observatory, the University of Minnesota, the University of California, and Goddard Space Flight Center with the support of NASA and the French Space Agency CNES. The authors want to thank the IMPACT, PLASTIC, and CDPP teams. The data from IMPACT, PLASTIC were obtained from the STEREO Sciences web page: http://stereo-ssc.nascom.nasa.gov/data/ins_data/, SIDC website: http://sidc.oma.be/silso/INFO/snytotcsv.php. "Fluctuat Nec Mergitur" is the Paris motto and it means *"It is tossed by the waves but does not sink."*

the differences between the distributions of E^{Max} and $E_{\parallel}^{\max}$). Seventy-seven percent of the database is composed of waves for which perpendicular components contribute to less than 10% to the total amplitude of the wave (i.e., Langmuir waves, blue crosses on Figure 9).

References

Bale, S. D., et al. (2008), The electric antennas for the STEREO/WAVES experiment, *Space Sci. Res.*, *136*, 529–547, doi:10.1007/s11214-007-9251-x.

Bougeret, J.-L., et al. (1995), Waves: The radio and plasma wave investigation on the wind spacecraft, *Space Sci. Rev.*, *71*, 231–263, doi:10.1007/BF00751331.

Bougeret, J. L., et al. (2008), S/WAVES: The radio and plasma wave investigation on the STEREO mission, *Space Sci. Rev.*, *136*, 487–528, doi:10.1007/s11214-007-9298-8.

Briand, C. (2015), Langmuir waves across the heliosphere, *J. Plasma Phys.*, *81*, 325810204, doi:10.1017/S0022377815000112.

Briand, C., et al. (2008), Faint solar structures from decametric observations, *Astron. Astrophys.*, *490*, 339–344, doi:10.1051/0004-6361:200809842.

Briand, C., J. Soucek, P. Henri, and A. Mangeney (2010), Waves at the plasma frequency inside magnetic holes: STEREO and CLUSTER observations, *J. Geophys. Res.*, *115*, A12113, doi:10.1029/2010JA015849.

Galvin, A. B., et al. (2008), The Plasma and Suprathermal Ion Composition (PLASTIC) investigation on the STEREO observatories, *Space Sci. Rev.*, *136*, 437–486, doi:10.1007/s11214-007-9296-x.

Graham, D. B., and I. H. Cairns (2013), Electrostatic decay of Langmuir/Z-mode waves in type III solar radio bursts, *J. Geophys. Res. Space Physics*, *118*, 3968–3984, doi:10.1002/jgra.50402.

Gurnett, D. A., R. L. Huff, and D. L. Kirchner (1997), The wide-band plasma wave investigation, *Space Sci. Res.*, *79*, 195–208, doi:10.1023/A:1004966823678.

Gurnett, D. A., et al. (2004), The Cassini radio and plasma wave investigation, *Space Sci. Res.*, *114*, 395–463, doi:10.1007/s11214-004-1434-0.

Henri, P., C. Briand, A. Mangeney, S. D. Bale, F. Califano, K. Goetz, and M. Kaiser (2009), Evidence for wave coupling in type III emissions, *J. Geophys. Res.*, *114*, A03103, doi:10.1029/2008JA013738.

Henri, P., N. Meyer-Vernet, C. Briand, and S. Donato (2011), Observations of Langmuir ponderomotive effects using the solar terrestrial relations observatory spacecraft as a density probe, *Phys. Plasmas*, *18*(8), 082308, doi:10.1063/1.3622667.

Khrabrov, A. V., and B. U. Ö. Sonnerup (1998), Error estimates for minimum variance analysis, *J. Geophys. Res.*, *103*, 6641–6652, doi:10.1029/97JA03731.

Luhmann, J. G., et al. (2008), STEREO IMPACT investigation goals, measurements, and data products overview, *Space Sci. Rev.*, *136*, 117–184, doi:10.1007/s11214-007-9170-x.

Malaspina, D. M., P. J. Kellogg, S. D. Bale, and R. E. Ergun (2010), Measurements of rapid density fluctuations in the solar wind, *Astrophys. J.*, *711*, 322–327, doi:10.1088/0004-637X/711/1/322.

Meyer-Vernet, N., and C. Perche (1989), Tool kit for antennae and thermal noise near the plasma frequency, *J. Geophys. Res.*, *94*, 2405–2415, doi:10.1029/JA094iA03p02405.

Nulsen, A. L., I. H. Cairns, and P. A. Robinson (2007), Field distributions and shapes of Langmuir wave packets observed by Ulysses in an interplanetary type III burst source region, *J. Geophys. Res.*, *112*, A05107, doi:10.1029/2006JA011873.

Opitz, A., et al. (2010), Temporal evolution of the solar wind electron core density at solar minimum by correlating the STEREO A and B SWEA measurements, *Sol. Phys.*, *266*, 369–377, doi:10.1007/s11207-010-9613-5.

Robinson, P. A. (1995), Stochastic wave growth, *Phys. Plasmas*, *2*, 1466–1479, doi:10.1063/1.871362.

Sonnerup, B. U. Ö., and M. Scheible (1998), Minimum and maximum variance analysis, in *Analysis Methods for Multi-Spacecraft Data, ISSI Sci. Rep. Ser.*, vol. 1, edited by G. Paschmann and P. W. Daly, pp. 185–220, Eur. Space Agency, Paris.

Stone, R. G., J. L. Bougeret, J. Caldwell, P. Canu, Y. de Conchy, N. Cornilleau-Wehrlin, M. D. Desch, J. Fainberg, K. Goetz, and M. L. Goldstein (1992), The unified radio and plasma wave investigation, *Astron. Astrophys. Suppl. Ser.*, *92*, 291–316.

Valentini, F., A. Vecchio, S. Donato, V. Carbone, C. Briand, J. Bougeret, and P. Veltri (2014), The nonlinear and nonlocal link between macroscopic Alfvénic and microscopic electrostatic scales in the solar wind, *Astrophys. J. Lett.*, *788*, L16, doi:10.1088/2041-8205/788/1/L16.

Vecchio, A., F. Valentini, S. Donato, V. Carbone, C. Briand, J. Bougeret, and P. Veltri (2014), Electrostatic fluctuations in the solar wind: An evidence of the link between Alfvénic and electrostatic scales, *J. Geophys. Res. Space Physics*, *119*, 7012–7024, doi:10.1002/2014JA020091.